

Nitrogen Doping Improves the Immobilization and Catalytic Effects of Co_9S_8 in Li-S Batteries

Yuping Liu, Shuangying Ma, Lifeng Liu, Julian Koch, Marina Rosebrock, Taoran Li, Frederik Bettels, Tao He, Herbert Pfnür, Nadja C. Bigall, Armin Feldhoff, Fei Ding, and Lin Zhang*

Several critical issues, such as the shuttling effect and the sluggish reaction kinetics, exist in the design of high-performance lithium–sulfur (Li-S) batteries. Here, it is reported that nitrogen doping can simultaneously and significantly improve both the immobilization and catalyzation effects of Co_9S_8 nanoparticles in Li-S batteries. Combining the theoretical calculations with experimental investigations, it is revealed that nitrogen atoms can increase the binding energies between LiPSs and Co_9S_8 , and as well as alleviate the sluggish kinetics of Li-S chemistry in the Li_2S_6 cathode. The same effects are also observed when adding N- Co_9S_8 nanoparticles into the commercial Li_2S cathode (which has various intrinsic advantages, but unfortunately a high overpotential). A remarkable improvement in the battery performances in both cases is observed. The work brings heteroatom-doped Co_9S_8 to the attention of designing high-performance Li-S batteries. A fundamental understanding of the inhibition of LiPSs shuttle and the catalytic effect of Li_2S in the newly developed system may encourage more effort along this interesting direction.

1. Introduction

The increasing demand for energy storage devices with high energy/power density, long cycle life as well as the low material cost has boosted the development of battery technology in recent years.^[1] Among the several most successful battery chemistries, Li-S battery has received significant attention due to its high theoretical specific capacity of 1672 mAh g^{-1} —about five times higher than the currently dominant lithium-ion battery. In addition, sulfur is naturally abundant, inexpensive, and environmentally friendly, making it an ideal choice as the battery electrode.^[2–5]

However, Li-S battery faces its own set of challenges. The most well-known issue is the uncontrolled dissolution of intermediate lithium polysulfides (LiPSs) into the electrolyte. This so-called “shuttling effect”

results in fast capacity fading and low Coulombic efficiency (CE).^[4,6] Another critical issue, which becomes a major focus in recent studies,^[7,8] is the sluggish redox kinetics of the insulating Li_2S during the electrochemical reactions. About 75% of the Li-S battery’s theoretical capacity comes from the transformation of soluble Li_2S_4 to solid Li_2S . Therefore, the catalysis of the decomposition of Li_2S and oxidization of Li_2S to Li_2S_x , and finally to sulfur are also crucial steps to realizing high capacity and CE.^[7] Therefore, innovative strategies need to be developed, which can take both issues into account.

Tremendous efforts have been devoted to improving the immobilization of polysulfide in Li-S batteries, mainly by physically constraining the sulfur within nanostructured carbon materials,^[9–13] or adding carbon interlayer for inhibiting the LiPSs dissolution in the electrolyte.^[14] But, the poor adsorption of the nonpolar carbon-based materials toward the LiPSs resulted in limited success.^[11,15] There are also research works that use the smaller sulfur molecules ($\text{S}_{2,4}$) in Li-S batteries to avoid the shuttle problem,^[16,17] however, the charge/discharge plateaus are relatively low in these works.

Recently, seminal results were reported on the introduction of heteroatoms into carbonaceous materials for the generation of polar functional groups to immobilize the LiPSs.^[18–21] Besides, a wide variety of other materials (beyond carbon-based materials) also show great promise in trapping LiPSs due to the similar polar interactions with LiPSs or the Lewis acid–base


Dr. Y. Liu, J. Koch, T. Li, F. Bettels, T. He, Prof. H. Pfnür,
Prof. F. Ding, Prof. L. Zhang
Institute for Solid State Physics
Leibniz University Hannover
Appelstrasse 2, Hannover 30167, Germany
E-mail: l.zhang@fkp.uni-hannover.de

Dr. Y. Liu, M. Rosebrock, T. Li, F. Bettels, T. He, Prof. H. Pfnür,
Prof. N. C. Bigall, Prof. F. Ding, Prof. L. Zhang
Laboratory of Nano and Quantum Engineering (LNQE)
Leibniz University Hannover
Schneiderberg 39, Hannover 30167, Germany

Dr. S. Ma
Institute for Theoretical Chemistry
University of Stuttgart
Pfaffenwaldring 55, Stuttgart 70569, Germany

Dr. L. Liu
International Iberian Nanotechnology Laboratory (INL)
Av. Mestre Jose Veiga, Braga 4715-330, Portugal

M. Rosebrock, Prof. N.-C. Bigall, Prof. A. Feldhoff
Institute of Physical Chemistry and Electrochemistry
Leibniz University Hannover
Callinstrasse 3a, Hannover 30167, Germany

 The ORCID identification number(s) for the author(s) of this article can be found under <https://doi.org/10.1002/adfm.202002462>.

© 2020 The Authors. Published by WILEY-VCH Verlag GmbH & Co. KGaA, Weinheim. This is an open access article under the terms of the Creative Commons Attribution License, which permits use, distribution and reproduction in any medium, provided the original work is properly cited.

DOI: 10.1002/adfm.202002462

interactions. For instance, metal oxide,^[22,23] metal sulfides,^[24–26] metal nitrides/carbides,^[27,28] and indium tin oxide.^[29] Very recently, single atoms are also reported as efficient catalysts for Li-S batteries.^[8,30]

Transition metal dichalcogenides (TMD),^[7,31–33] on the other hand, are interesting in Li-S batteries mainly due to that the metal d-orbitals and unsaturated heteroatoms (such as S) result in an effective d-band structure with catalytic characteristics. Their catalytic activities for the LiPSs are correlated to the exposed edge sites.^[31,34] Although they can improve the Li-S battery performance to a certain extent (when compared with pure S or Li₂S₆), the results are far from satisfactory.

In this work, we report that nitrogen (N) doping can improve, simultaneously, both the LiPSs immobilization and the redox catalyzation capabilities of Co₉S₈ nanoparticles in Li-S batteries. This is because, on the one hand, N doping is an efficient approach to optimize the electrochemical performances in Li-S batteries, by reducing the intrinsic activation barriers during the catalytic reactions.^[35–37] And on the other hand, Li–N bonds are more favorable than Li–S bonds when anchoring LiPSs in Li-S batteries.^[38,39] Density functional theory (DFT) calculations provide an insight into the strong chemical bonding between the LiPSs and the surface of N-Co₉S₈ nanoparticles. Further supported by experiments, we conclude that N atoms significantly increase the binding energies and hence help to prevent the LiPSs shuttling.

When compared with the undoped Co₉S₈ (in Li₂S₆ cathodes), the N-doped Co₉S₈ shows significant improvements in the battery performances. The polarization is lower, the capacity is improved (1233 mAh g⁻¹ at 0.2 A g⁻¹), the redox reaction is faster (604 mAh g⁻¹ at 20 A g⁻¹), the capacity retention is better (decay of 0.037%/cycle over 1000 cycles), and the sulfur utilization is higher. The results at high mass loading (up to 5 mg cm⁻²) and high current densities (up to 20 A g⁻¹) are also excellent.

Furthermore, N-Co₉S₈ nanoparticles are also tested as an additive to the commercial Li₂S in cathodes. We observe a much reduced potential barrier and a much larger specific capacity. This suggests a viable route to construct a Li₂S-based Li-S battery that has several intrinsic advantages.^[40] For example, since the lithium is stored in Li₂S, the lithium metal anode can be replaced by a high capacity silicon anode to avoid the dendrite problem and the low CE issue. Also, as the least-dense phase of the sulfur-containing species, no volume expansion is expected for the Li₂S-based cathodes during the cell operations. Therefore, our work on the novel N-doped Co₉S₈ material may open a new avenue for designing practical Li-S batteries and encourage more efforts along this interesting direction.

2. Results and Discussion

2.1. N-Co₉S₈ Structural and Morphology Analysis

N-Co₉S₈ nanoparticles were synthesized through the hydrothermal reactions (see Experimental Section). The as-fabricated N-Co₉S₈ nanoparticles were first investigated by the X-ray diffraction (XRD) to determine its crystalline structure, and

all the diffraction peaks are assignable to the face-centered cubic structure of Co₉S₈ (JCPDS card number: 01-073-6395) without any noticeable impurity phase (**Figure 1a**). The detailed morphology, structure, and composition of the products were studied by the scanning electron microscopy (SEM) and the transmission electron microscopy (TEM). As shown in **Figure 1b,c**, all N-Co₉S₈ nanoparticles show a well-defined spherical nanostructure with a diameter of around 40 nm, and therefore have large surface areas and abundant adsorption/catalytic active sites. The N-Co₉S₈ nanoparticles, both after being coating on carbon paper and after the addition of Li₂S₆, show a uniform distribution, as shown in **Figure S1**, Supporting Information. The energy-dispersive X-ray spectrum (EDXS) elemental mappings (**Figure 1d–g**) show that the spatial distributions of the N, Co and S atoms are highly correlated over the entire nanoparticles.

X-ray photoelectron spectroscopy (XPS) measurements were performed in order to confirm the successful N-doping of the Co₉S₈ nanoparticles (**Figure 1h–j**). The Co 2p signal consists of a Co 2p_{3/2} and a Co 2p_{1/2} component, each of which can be further deconvoluted into the Co³⁺ (776.8 and 791.9 eV), Co²⁺ (779.4 and 794.9 eV), and the satellite (784.1 and 801.0 eV) peaks.^[36,41,42] The satellite peaks are due to the plasmon or shake-up losses, since their energy shifts are too large to be explained by a chemical shift. In particular, they cannot be due to bonds to O atoms as suggested in ref. [31]. Such peaks would overlap with the peaks resulting from the bonds to the S atoms. The S 2p spectrum shows a peak at 160.8 eV associated with S²⁻, and a peak at 166.4 eV that is most likely due to the sulfite species.^[43] Finally, the N 1s peak located at 398.5 eV confirms the presence of the N-Co species and the successful N-doping.^[36] From the XPS analysis, the N concentration is approximately 5 at%. The undoped Co₉S₈ nanoparticles show a similar structure and morphology to that of the N-Co₉S₈ nanoparticles, as shown in **Figure S2**, Supporting Information.

2.2. LiPSs Adsorption

First, we have performed DFT calculations to investigate the interaction between the LiPSs and the surface of Co₉S₈/N-Co₉S₈ nanoparticles. The goal is to evaluate the binding energies quantitatively between the two species. From the texture in XRD measurements, we know that the (311) and (440) surfaces are two main facets for both N-Co₉S₈ and Co₉S₈ nanoparticles. Therefore, the first-principles calculations were performed to study the adsorbed structures and adsorption energies of the two typical LiPSs (Li₂S₂ and Li₂S₄, because of the capacity contribution in Li-S battery is mainly from this low-order LiPSs) on the (311) and (440) surfaces of Co₉S₈. From the adsorption structures (**Figure 2a,b**; **Figure S3**, Supporting Information), it is clear that the Li and S atoms of LiPSs chemically bonds with the S and Co atoms on the surfaces of Co₉S₈. Interestingly, after the surface doping with nitrogen atoms, the Li atoms tend to bond with the N atoms. This is confirmed by the formation of Li–N bonds in the XPS analysis (**Figure S4**, Supporting Information).

The binding energy E_{ads} between Co₉S₈ and Li₂S₂ on the (311) and (440) surfaces are 3.66 eV and 5.94 eV, respectively.

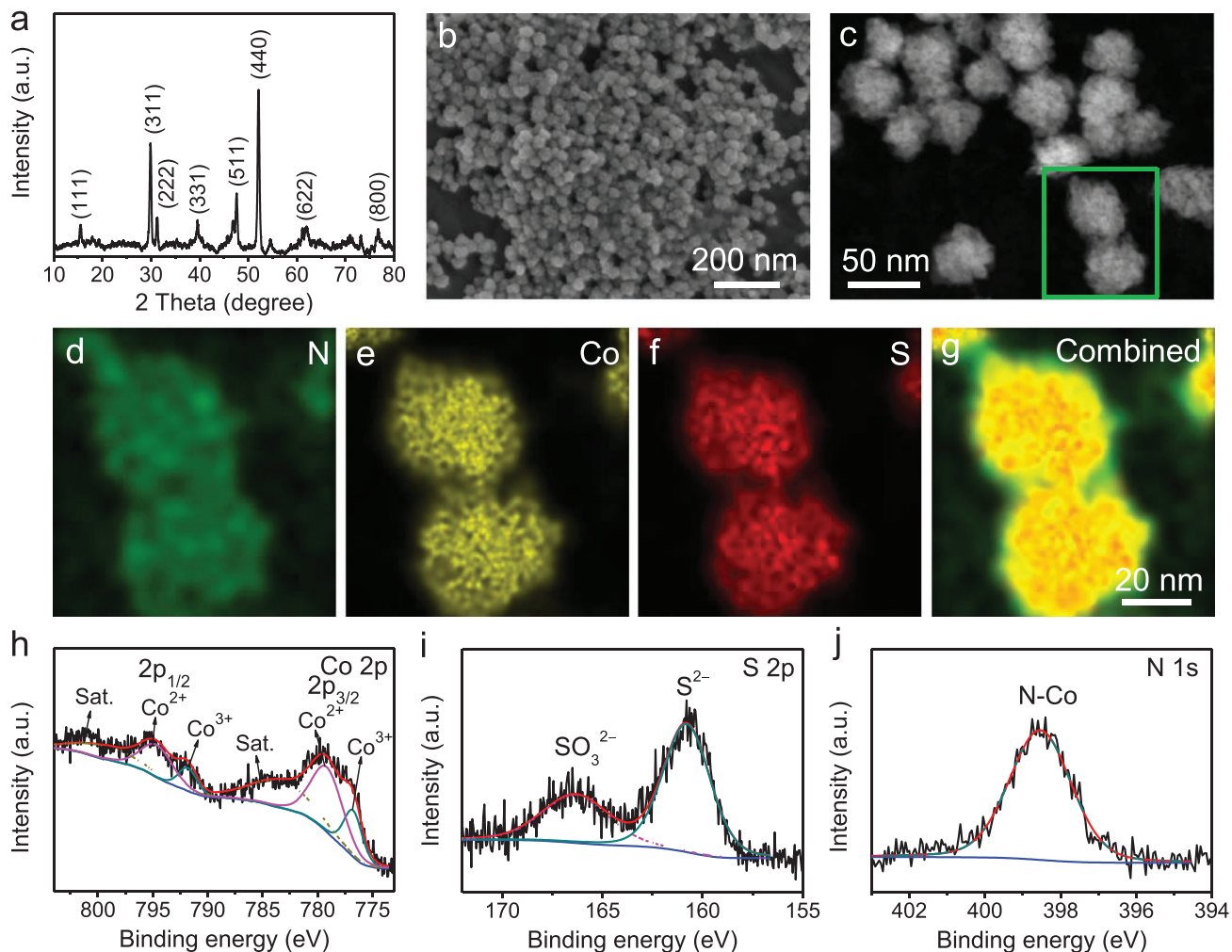


Figure 1. Structural and morphological characterizations of the N-Co₉S₈ nanoparticles. a) XRD pattern, b) SEM, c) HAADF-STEM. EDXS elemental maps of d) N, e) Co, f) S, and g) their combination for the N-Co₉S₈ nanoparticles. XPS analysis of the h) Co 2p spectrum, the i) S 2p spectrum, and j) N 1s spectrum.

For Li₂S₄ on the (311) and (440) surfaces, E_{ads} are 3.0 eV and 4.87 eV, respectively. After the N-doping, the E_{ads} of Li₂S₂ on the (311) and (440) surfaces are 11.01 eV and 6.15 eV, and Li₂S₄ on the (311) and (440) surfaces are 12.66 eV and 6.064 eV, respectively (Figure 2c). The E_{ads} of LiPSs is increased (by more than three times in case of the (311) surface) after N-doping, indicating a more energetically favourable and stronger chemical anchoring of N-Co₉S₈ nanoparticles to the LiPSs. We want to emphasize that this effect was not seen in the typical TMD structures, and it contributes to the greatly enhanced performances of the Li-S battery presented here.

The DFT calculation results (Figure 2c) are strongly supported by the experimental results. Figure 2d shows the adsorption ability of N-Co₉S₈ and Co₉S₈ nanoparticles in the Li₂S₆ solution. A significant color change was observed after adding N-Co₉S₈ nanoparticles, indicating strong physical adsorption. The Co₉S₈ nanoparticles, on the other hand, show lower adsorption capability and the Li₂S₆ solution showed only a light yellow color after 6 h (Figure 2d). Ultraviolet/visible spectroscopy was

also performed, in order to demonstrate the concentration changes of Li₂S₆ solutions after adding the N-Co₉S₈ or Co₉S₈ nanoparticles, respectively. Consistent with the physical adsorption results, the absorption peak of Li₂S₆ is reduced remarkably after adding the N-Co₉S₈ nanoparticles (Figure S5, Supporting Information).

The DFT calculations, together with the LiPSs absorption experiments, prove that the notorious “shuttling effect” is inhibited by the N-doped Co₉S₈ nanoparticles, which has not been reported by previous works. Now, the question is whether another critical issue—the sluggish redox kinetics, is also alleviated by our design. As shown already in a few reports,^[7,31] TMD materials can enhance the Li-S battery performances, to a certain extent, when compared with the pure S or Li₂S₆. These results are still far from satisfactory, especially when considering the practical conditions of high mass loadings and high rates. In the following, we show strong evidence that the nitrogen doping drastically improves the performances of Co₉S₈-based electrodes in Li-S batteries.

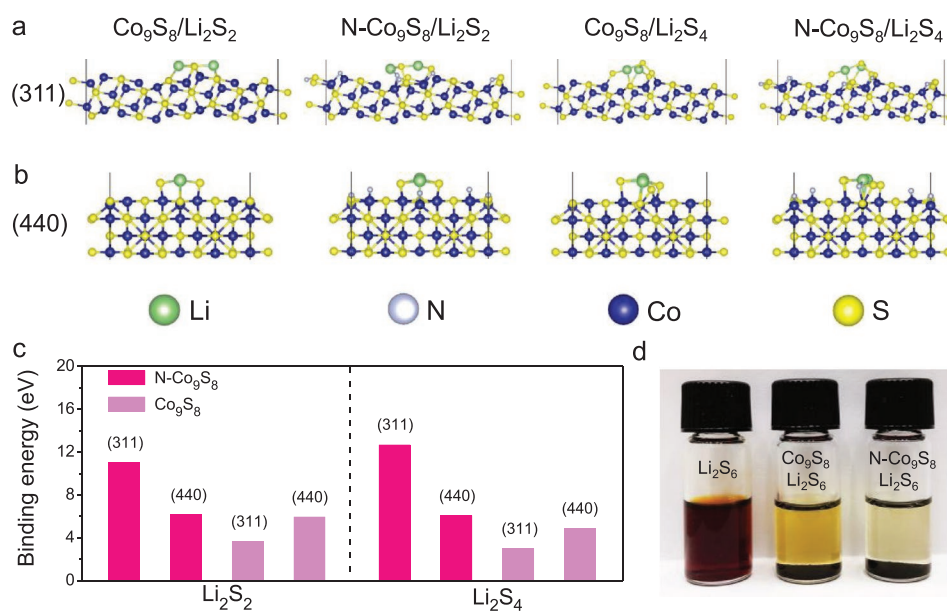


Figure 2. Illustrations of the interactions between LiPSs and the surfaces of Co₉S₈ and N-Co₉S₈ nanoparticles, respectively. Top view of optimized configurations on the a) (311) and b) (440) surfaces, respectively, c) DFT calculation shows a significant increase in binding energies due to the N doping, d) LiPSs adsorption ability of N-Co₉S₈ and Co₉S₈ nanoparticles in the Li₂S₆ solution.

2.3. LiPSs Anchoring–Diffusion–Conversion Processes

Figure 3a–c shows the schematics of LiPSs anchoring–diffusion–conversion processes on the N-Co₉S₈, Co₉S₈ electrodes and on a pure carbon paper. In order to investigate the mechanisms behind these processes, we first performed experiments with the N-Co₉S₈/Li₂S₆, Co₉S₈/Li₂S₆, and pure Li₂S₆ cathodes, respectively. Cyclic voltammetry (CV) tests were used to reveal the electrocatalytic activities of N-Co₉S₈ nanoparticles for the charge transfer to LiPSs. As shown in Figure 3d, there are two pairs of distinct and reversible redox peaks for the N-Co₉S₈/Li₂S₆ cathode. The reduction peaks at 2.35 V and 2.1 V belong to the transition from sulfur (S₈) to high-order LiPSs (Li₂S_χ, 4 ≤ χ ≤ 8), and then high-order LiPSs to Li₂S₂/Li₂S, respectively. In the reverse oxidation process, two anodic peaks at 2.35 V and 2.4 V are related to the transition from solid Li₂S₂/Li₂S to LiPSs, and then to Li₂S₈/S₈.^[44,45] These cathodic/anodic peak positions are consistent with the previously reported results. In the first three cycles, there are almost no peak shifts, indicating that the formation of sulfur species in the N-Co₉S₈/Li₂S₆ chemistry is completely reversible.^[46,47] The CV curves of the Co₉S₈/Li₂S₆ cathode are similar to those of the N-Co₉S₈/Li₂S₆ cathode (Figure 3e). On the other hand, the redox peaks for the pure Li₂S₆ cathode are significantly broader and only one reduction peak can be observed, which suggests a sluggish kinetic process during charging/discharging (Figure 3f).

When comparing the peak potentials of these three electrodes (Figure 3g), it is clear that the N-Co₉S₈/Li₂S₆ cathode has the highest reduction potential and the lowest oxidation potential, and then followed by the Co₉S₈/Li₂S₆ cathode and the pure Li₂S₆ cathode. This indicates that the N-Co₉S₈ nanoparticles can reduce the polarization, which is due to their electrocatalytic effect for the S/Li₂S during the charge/discharge processes.^[47,48] Similar result is also observed for the onset

potentials (Figure 3h). For the onset potential values of the cathodic peaks R₁ and R₂: N-Co₉S₈/Li₂S₆ > Co₉S₈/Li₂S₆ > pure Li₂S₆. For the anodic peaks O₁ and O₂: N-Co₉S₈/Li₂S₆ < Co₉S₈/Li₂S₆ < pure Li₂S₆.

More interestingly, when comparing the peak currents (Figure 3i), it is found that the N-Co₉S₈/Li₂S₆ cathode exhibits the largest current densities in both the cathodic and anodic processes. The peak currents of the cathodic peak O₁ (O₂) for N-Co₉S₈ is about 40% (36%) larger than that for Co₉S₈, and nearly 240% (146%) larger than that for the pure Li₂S₆. This is a strong evidence that N-Co₉S₈ nanoparticles can significantly improve the sluggish electron transfer to LiPSs, and hence the redox rate of Li-S chemistry during charge/discharge.

2.4. Electrochemical Performances

The nitrogen doping simultaneously improves the immobilization and the catalytic effects of the Co₉S₈ nanoparticles. As a result, the Li-S batteries based on the N-Co₉S₈/Li₂S₆ cathode show unprecedented electrochemical performances. Figure 4a shows the first three galvanostatic charge/discharge curves of the N-Co₉S₈/Li₂S₆ cathode at a current density of 0.2 A g⁻¹ within a potential window of 1.7–2.8 V (Li₂S₆, corresponding to ≈1 mg cm⁻² of S), and the curves are constant with the previous reports on the Li-S batteries based on other hosts.^[8,32,49]

The charge/discharge curves of Co₉S₈/Li₂S₆ and Li₂S₆ cathodes (with the same S mass loading) are shown in Figure S6, Supporting Information. All these three cathodes display two typical discharge plateaus, which indicate the multistep reduction reactions of sulfur during the discharge process. The high plateau (≈2.35 V) is attributed to the transformation from S₈ to the high order LiPSs (Li₂S_χ, 4 ≤ χ ≤ 8), while the low plateau

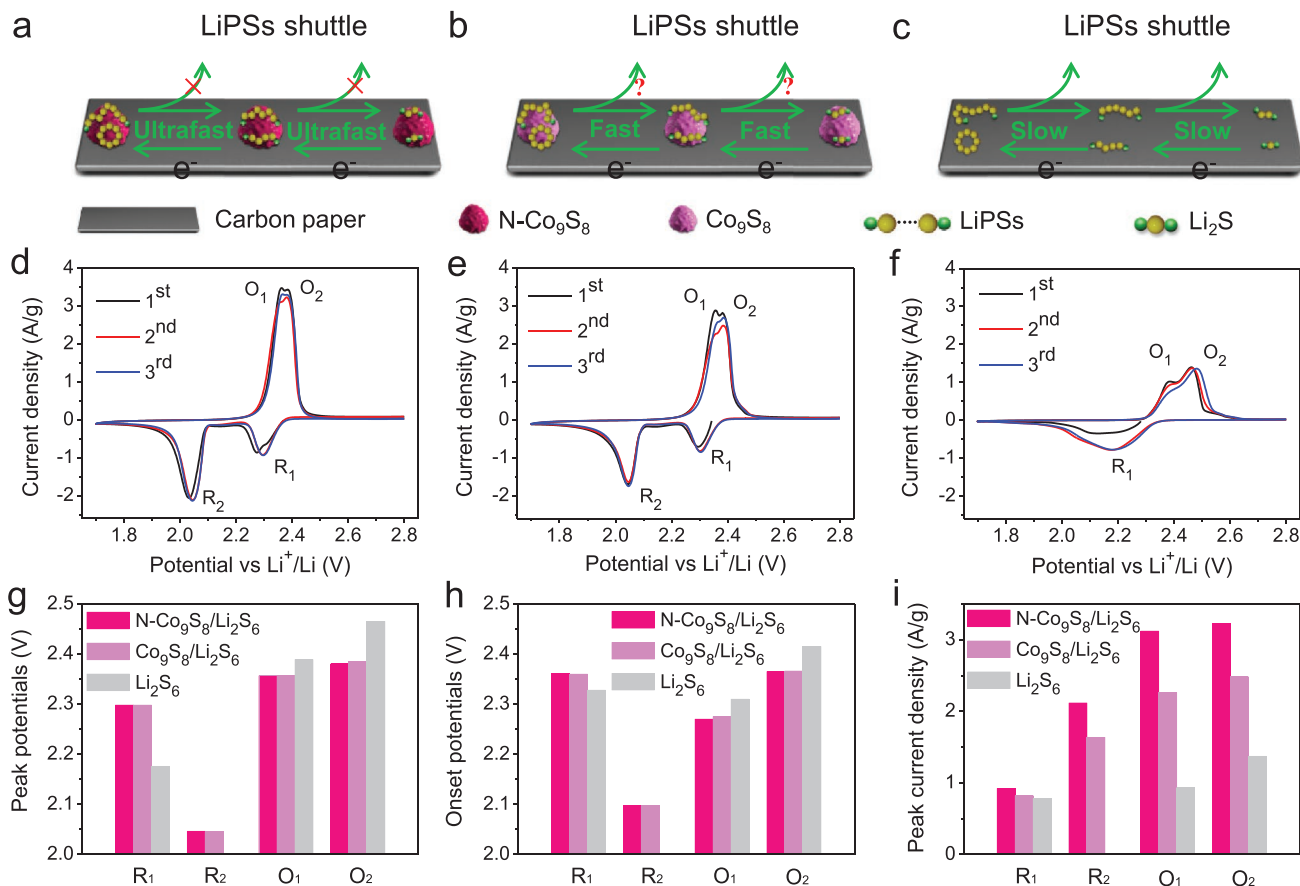


Figure 3. Schematics of the LiPSs anchoring–diffusion–conversion processes on the a) N-Co₉S₈, b) Co₉S₈ electrodes, and c) on a pure carbon paper. CV curves for the d) N-Co₉S₈/Li₂S₆, e) Co₉S₈/Li₂S₆, and f) Li₂S₆ cathodes are shown at a scan rate of 0.1 mV s⁻¹ in a potential window from 1.7 to 2.8 V (R, reduction peak; O, oxidation peak). The corresponding g) peak potentials, h) onset potentials, and i) peak current density are shown in the second CV cycle.

(≈2.1 V) is related to the reduction of high order LiPSs to Li₂S₂/Li₂S. The plateaus in charge profiles are due to the conversions from Li₂S₂/Li₂S to S₈.^[44,45]

Although these three cathodes have similar charge/discharge profiles, the specific capacity of N-Co₉S₈/Li₂S₆ cathode is much larger than that of the Co₉S₈/Li₂S₆ and the pure Li₂S₆ cathodes (especially during the low potential plateau ≈2.1 V, as shown in Figure 4b). This proves that the LiPSs dissolution and the shuttle effects have been effectively suppressed by the N-Co₉S₈ nanoparticles, thus leading to a high utilization rate of LiPSs. A similar effect is also observed in the SEM (EDXS elemental maps) of the Li anode after three cycles (Figure S7, Supporting Information). Again, these results give a strong evidence that the active N-doping in N-Co₉S₈ nanoparticles can effectively immobilize the LiPSs, therefore suppressing the “shuttling effect” in Li-S batteries. Furthermore, when comparing the polarizations of the charge/discharge profiles in the second cycle (Figure 4c), it is clear that the N-Co₉S₈/Li₂S₆ cathode shows a much lower polarization value (131 mV) than that of the Co₉S₈/Li₂S₆ cathode (175 mV) and the pure Li₂S₆ cathode (225 mV). This suggests a more kinetically efficient reaction process due to the nitrogen doping. These results agree very well with the CV results in Figure 3.

To further investigate the electrochemical performances, these three electrodes were cycled at varied current densities of 0.2, 1, 2, 5, 10, and 20 A g⁻¹. The N-Co₉S₈/Li₂S₆ cathode delivered a stable discharge capacity of 1233 mAh g⁻¹, 1096 mAh g⁻¹, 1009 mAh g⁻¹, 864 mAh g⁻¹, 730 mAh g⁻¹, and 604 mAh g⁻¹, respectively (Figure 4d). The two typical plateaus in the charge and discharge curves are clear and stable, even at the largest current density of 20 A g⁻¹. And after the current density returned to 0.2 A g⁻¹, the reversible specific capacity was recovered to 1010 mAh g⁻¹ (Figure 4e). The stable charge/discharge plateaus, together with the excellent reversibility, confirm that the N-Co₉S₈ nanoparticles can effectively immobilize the LiPSs and accelerate the electron transfer to LiPSs even at high current densities. In stark contrast, the Co₉S₈/Li₂S₆ cathode and pure Li₂S₆ cathode (especially, the latter) exhibited much lower rate capacities under the same conditions (Figure 4e). We observe the rate performance of N-Co₉S₈/Li₂S₆ cathode represents a very high level when compared with that of the previously reported Li-S batteries. Especially under large current densities (≥5 A g⁻¹), the capacities are the highest among all available reports (Figure 4f).^[50–56]

For many applications (such as in electric vehicles), a high cycling rate with a high mass loading of active material is

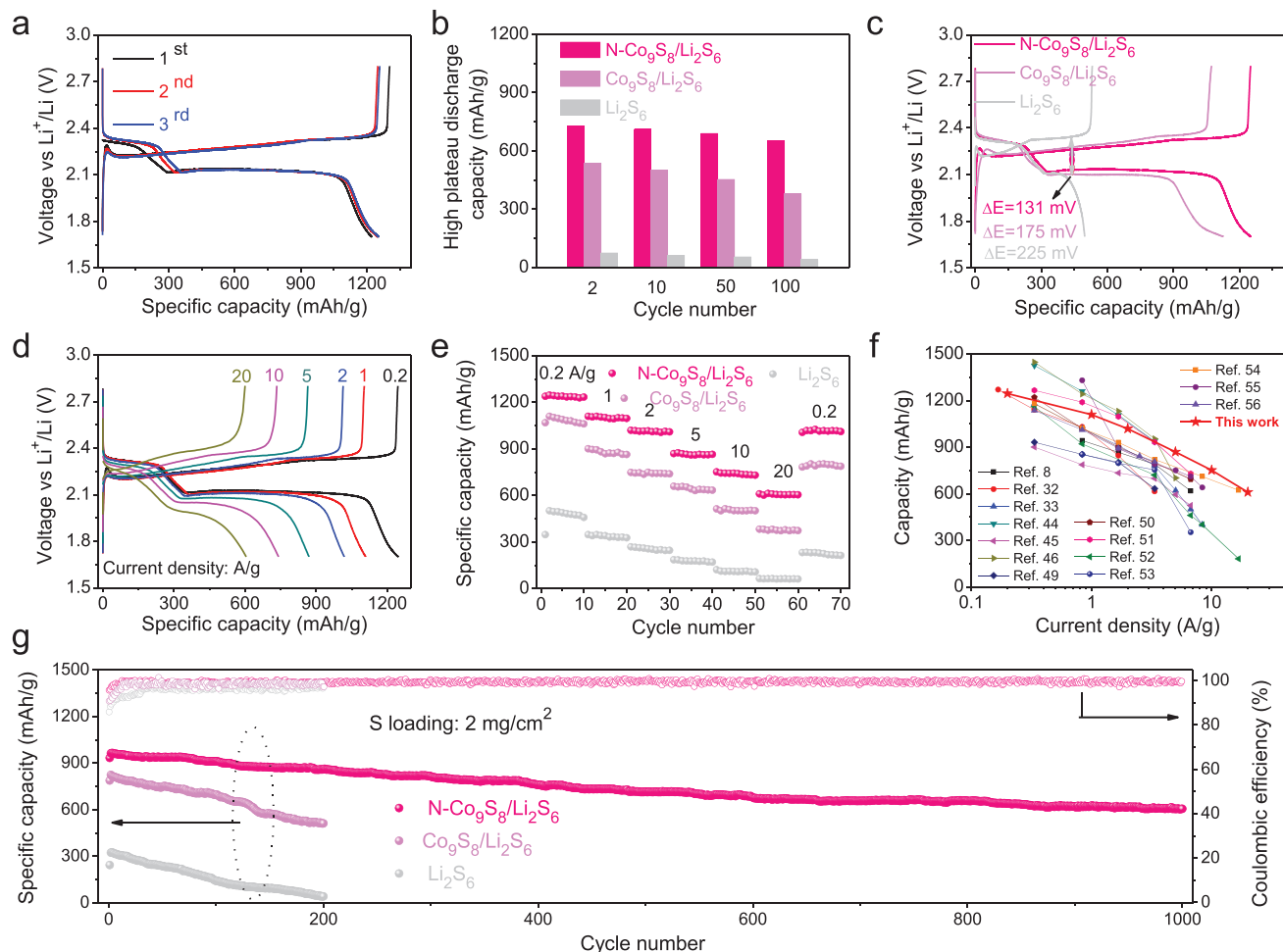


Figure 4. Electrochemical performances of the Li-S batteries. a) Typical charge/discharge profiles of the N-Co₉S₈/Li₂S₆ cathode for the first three cycles at 0.2 A g⁻¹, b) High plateau discharge capacity of the N-Co₉S₈/Li₂S₆, Co₉S₈/Li₂S₆, and Li₂S₆ cathodes in the 2nd, 10th, 50th, and 100th cycle, c) charge/discharge profiles of the N-Co₉S₈/Li₂S₆, Co₉S₈/Li₂S₆, and Li₂S₆ cathodes in the second cycle, d) charge/discharge profiles of the N-Co₉S₈/Li₂S₆ cathode at various current densities of 0.2–20 A g⁻¹, e) rate capability of the N-Co₉S₈/Li₂S₆, Co₉S₈/Li₂S₆, and Li₂S₆ cathodes at various current densities of 0.2–20 A g⁻¹, f) comparison of the rate capability of N-Co₉S₈/Li₂S₆ cathode with that of Li-S batteries from recent publications, g) cycling stability of the N-Co₉S₈/Li₂S₆, Co₉S₈/Li₂S₆, and Li₂S₆ cathodes with 2 mg cm⁻² S mass loading cycled at 1 A g⁻¹ for 1000 cycles.

critical. Figure 4g shows the long-term performance of these three cathodes with a high mass loading (S: 2 mg cm⁻²) cycled at 1 A g⁻¹. After 1000 cycles, the N-Co₉S₈/Li₂S₆ cathode delivered a specific capacity of 605 mAh g⁻¹—with only 0.037% capacity decay per cycle on average, and maintained a high CE (average CE ≈98.5%). In the meanwhile, both Co₉S₈/Li₂S₆ and pure Li₂S₆ cathodes showed not only significantly lower capacities but also a much faster capacity decay. For example, when compared with Co₉S₈/Li₂S₆ (pure Li₂S₆) at the 200th cycle, the newly developed N-Co₉S₈/Li₂S₆ showed 174% (250%) improvement in the specific capacity.

Considering the theoretical capacity of sulfur, the sulfur utilization for the N-Co₉S₈/Li₂S₆ cathode is greater than that of the Co₉S₈/Li₂S₆ and Li₂S₆ cathodes (Figure S8, Supporting Information). Moreover, the cycling performance of the N-Co₉S₈/Li₂S₆ cathode with an even higher S mass loading (≈5 mg cm⁻²) was also tested. It showed an ultrahigh specific capacity of 870 mAh g⁻¹ (cycled at 1 A g⁻¹) and >600 mAh g⁻¹ was remained after 300 cycles (Figure S9, Supporting Information). This

unprecedented performance at high rates with high mass loading suggests the strong potential of N-Co₉S₈ nanoparticles for use in practical Li-S batteries.

2.5. Catalytic Oxidation of Li₂S

Encouraged by the excellent performances of our newly developed N-Co₉S₈ nanoparticles, we tested the commercial Li₂S as cathode for Li-S battery. There are several intrinsic advantages of Li₂S-based Li-S batteries, such as the inhibition of volume expansion during cell operations and the possibility of using non-lithium-metal anodes. However, it is known that Li₂S suffers from a low Li-ion diffusivity, low electrical conductivity, and high charge transfer resistance, which result in a high overpotential during the initial charging.^[7] Here, we mixed the commercial Li₂S with N-Co₉S₈ nanoparticles, carbon black, and PVDF to prepare the cathodes (see Experimental Section). The assembled coin cells were first charged to 4.0 V from

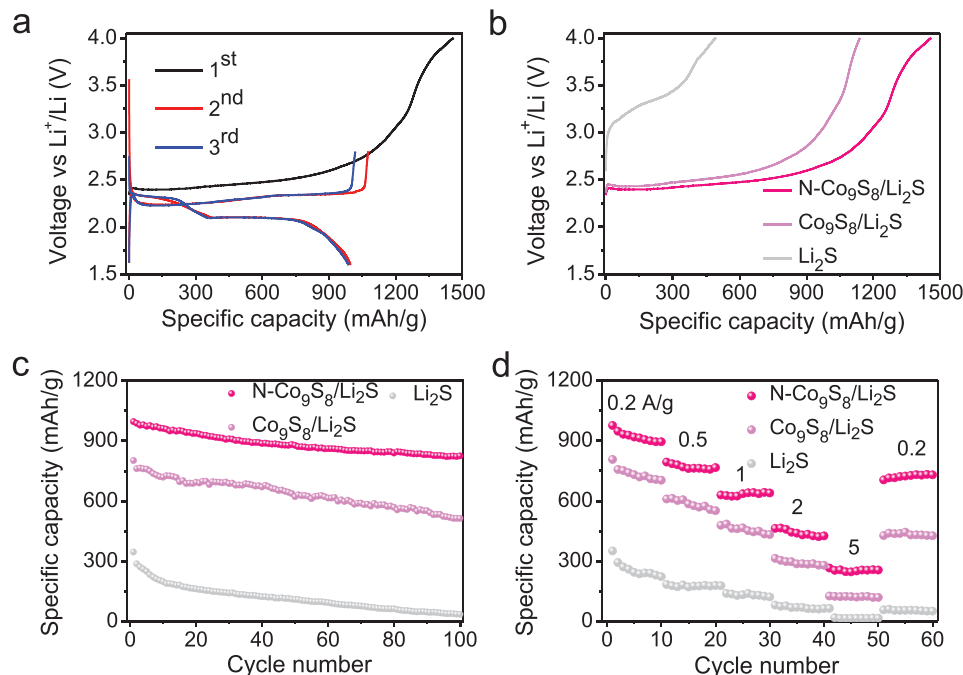


Figure 5. Catalytic oxidation of the commercial Li_2S in cathode. a) Typical charge/discharge profiles N- $\text{Co}_9\text{S}_8/\text{Li}_2\text{S}$ cathode for the first three cycles at 0.2 A g^{-1} , b) first charge voltage profiles of N- $\text{Co}_9\text{S}_8/\text{Li}_2\text{S}$, $\text{Co}_9\text{S}_8/\text{Li}_2\text{S}$, and Li_2S cathodes, c) cycling stability of N- $\text{Co}_9\text{S}_8/\text{Li}_2\text{S}$, $\text{Co}_9\text{S}_8/\text{Li}_2\text{S}$, and Li_2S cathodes at 0.2 A g^{-1} for 100 cycles, d) rate capability of N- $\text{Co}_9\text{S}_8/\text{Li}_2\text{S}$, $\text{Co}_9\text{S}_8/\text{Li}_2\text{S}$, and Li_2S cathodes at various current densities of $0.2\text{--}5 \text{ A g}^{-1}$.

open-circuit to delithiate Li_2S , with the aim to convert Li_2S to the low-order LiPSs, high-order LiPSs and finally S .^[40,57]

Figure 5a shows the first three cycles of N- $\text{Co}_9\text{S}_8/\text{Li}_2\text{S}$ cathode. After the initial delithiation of Li_2S , the following cycles show curves that are similar to that of a typical Li-S battery. The charge/discharge curves for the $\text{Co}_9\text{S}_8/\text{Li}_2\text{S}$ and pure Li_2S cathodes can be found in Figure S10, Supporting Information. Figure 5b shows the initial delithiation of Li_2S in these three different cathodes, and the pure Li_2S electrode exhibits a high potential barrier until 4.0 V , indicating a sluggish activation process and a high charge transfer resistance. Interestingly, the N- $\text{Co}_9\text{S}_8/\text{Li}_2\text{S}$ cathode shows a voltage jump after a relatively higher initial potential barrier and maintains a long charge plateau at $\approx 2.5 \text{ V}$. This is an indication of a strongly reduced charge transfer resistance due to the catalytic effect of nitrogen doping. It is worth mentioning that this potential barrier is much lower than that in the previous reports.^[57,58] A similar charging phenomenon is observed for the $\text{Co}_9\text{S}_8/\text{Li}_2\text{S}$ cathode, but with a higher potential barrier and a smaller specific capacity. Electrochemical impedance spectra (EIS) measured at the open-circuit voltage also support the reduced charge transfer resistance in the N- $\text{Co}_9\text{S}_8/\text{Li}_2\text{S}$ cathode (Figure S11, Supporting Information).^[59,60] And from EIS, the diffusion coefficient of Li^+ ions in N- $\text{Co}_9\text{S}_8/\text{Li}_2\text{S}$, $\text{Co}_9\text{S}_8/\text{Li}_2\text{S}$, and Li_2S electrodes at their initial state is calculated to be $6.7 \times 10^{-11} \text{ cm}^2 \text{ s}^{-1}$, $8.4 \times 10^{-12} \text{ cm}^2 \text{ s}^{-1}$, and $7.6 \times 10^{-15} \text{ cm}^2 \text{ s}^{-1}$, respectively.^[61] It is clear that the value in the N- $\text{Co}_9\text{S}_8/\text{Li}_2\text{S}$ electrode is nearly four orders of magnitude higher than that in the pure Li_2S electrode. Therefore, the N- Co_9S_8 nanoparticles can facilitate an efficient migration of Li^+ thus accelerate the transformation of Li_2S or S_8 . All these electrocatalytic measurement results are consistent with that of the Li_2S_6 cathodes shown above.

The cycling performances of the commercial Li_2S -based cathodes are shown in Figure 5c. The N- $\text{Co}_9\text{S}_8/\text{Li}_2\text{S}$ cathode delivers an excellent discharge capacity of 825 mAh g^{-1} after 100 cycles. On the contrary, the $\text{Co}_9\text{S}_8/\text{Li}_2\text{S}$ and Li_2S cathodes show a rapid capacity decay. The rate capability shows a similar result (Figure 5d). It is worth mentioning that the contributions of N- Co_9S_8 or Co_9S_8 to the total capacity can be neglected (Figure S12, Supporting Information). We envision that, thanks to the excellent results of N- $\text{Co}_9\text{S}_8/\text{Li}_2\text{S}$ cathode, a safe Li-S full battery can be built by pairing the new cathode with an Si or C anode (instead of the highly active lithium metal). Also, it can lead to a much higher specific energy when compared with the commercial $\text{LiCoO}_2/\text{graphite}$ system.^[62,63]

3. Conclusion

We demonstrate that nitrogen-doped Co_9S_8 nanoparticles are a highly attractive material for Li-S batteries. Combining the theoretical calculations with the experimental results, we prove that the nitrogen doping can simultaneously and significantly improve the immobilization and the catalyzation of the polysulfides by the Co_9S_8 nanoparticles. We observe an effective suppression of the shuttling behavior, and as well as a significant acceleration of the redox reaction kinetics. As a result, the N- Co_9S_8 nanoparticles/ Li_2S_6 composite cathodes exhibit a high reversible capacity (1245 mAh g^{-1} at 0.2 mA g^{-1}), fast reaction kinetics (a record value of 604 mAh g^{-1} at 20 A g^{-1}), as well as a low capacity decay of $0.037\%/ \text{cycle}$ over 1000 cycles. The excellent performances are retained even at high mass loadings (up to 5 mg cm^{-2}) and high current densities. A proof-of-concept experiment is also shown: the N- Co_9S_8 nanoparticles were

mixed with commercial Li_2S and used as cathodes. To conclude, we report that the nitrogen-doped Co_9S_8 nanoparticles can solve the two main challenges (the “shutting effect” and the sluggish redox kinetics) in Li-S batteries, and thus dramatically improve the battery performances. Our work may encourage more efforts along this interesting direction.

4. Experimental Section

Materials: Cobalt (II) nitrate hexahydrate ($\text{Co}(\text{NO}_3)_2 \cdot 6\text{H}_2\text{O}$), thioacetamide (CH_3CSNH_2), polyvinylpyrrolidone (PVP), sodium hydroxide (NaOH), sulfur powder (S), lithium sulfide (Li_2S), and lithium nitrate (99.99% trace metals basis) were purchased from Sigma-Aldrich. Urea (ACS, 99.0–100.5%) was purchased from Alfa Aesar. All these chemicals were used as received without any further purification.

Synthesis of N-Doped Co_9S_8 Nanoparticles: N-doped Co_9S_8 nanoparticles were synthesized through a simple hydrothermal reaction. Briefly, 1.746 g $\text{Co}(\text{NO}_3)_2 \cdot 6\text{H}_2\text{O}$, 0.9 g CH_3CSNH_2 , and 0.42 g PVP were dissolved in 300 mL distilled water and stirred to form a homogeneous solution, then 72 mL 0.5 M NaOH was added into this solution. The mixture was transferred to a three-necked flask and heated to 100 °C with a heating rate of 5 °C min^{-1} under nitrogen atmosphere and stirred for 2 h. Then, 0.03636 g urea (as nitrogen source) was added into this solution, which was kept at 100 °C for another 30 min. After cooling, the product was washed with ethanol for three times, and then dried using a freeze dryer. For comparison, Co_9S_8 nanoparticles were synthesized using a similar approach but without adding urea.

Preparation of the Li_2S_6 Catholyte: Sulfur and Li_2S at a molar ratio of 5:1 were added to an appropriate amount of 1,3-dioxolane (DOL) and 1,2-dimethoxyethane (DME) by vigorous magnetic stirring at 50 °C overnight in the glove box in order to obtain 1 M lithium polysulfide (Li_2S_6) catholyte.

Polysulfide Adsorption Test: Li_2S_6 solution was diluted to a concentration of 10 mmol L^{-1} (calculated based on the S content). Then the N- Co_9S_8 and Co_9S_8 nanoparticles powders were added to the Li_2S_6 solution (with a mass ratio of 2:8), respectively. The mixtures were stirred and then waited for 6 h to ensure a thorough adsorption process. The glass vial only with Li_2S_6 solution was used for comparison.

Materials Characterization: XRD patterns of the N- $\text{Co}_9\text{S}_8/\text{Co}_9\text{S}_8$ nanoparticles were recorded by using $\text{Cu-K}\alpha$ radiation on a Bruker D8 Advance Discovery X-ray Diffractometer. The morphology, microstructure, and composition of the N- $\text{Co}_9\text{S}_8/\text{Co}_9\text{S}_8$ nanoparticles were investigated by the emission scanning electron microscopy (FE-SEM, JEOL JSM-6700F) and transmission electron microscopy (FEI, ChemiSTEM 80–200, C_c -corrected) under the high-angle annular dark-field scanning transmission electron microscopy (HAADF-STEM) mode, operated at 200 kV. XPS analysis was performed with a hemispherical analyzer of 100 mm radius (Leybold Heraeus). Ultraviolet/visible absorbance spectroscopy was performed in the spectral range of 200–800 nm using a Cary 5000 UV–vis variable wavelength spectrophotometer to evaluate the lithium polysulfide absorption capability of N- Co_9S_8 and Co_9S_8 nanoparticles.

Electrochemical Measurements: N- Co_9S_8 or Co_9S_8 nanoparticles were mixed with polyvinylidene difluoride (PVDF) in N-methyl-2-pyrrolidone (9:1 by weight) by vigorous magnetic stirring to form a homogeneous slurry, respectively. It was subsequently blade coated onto the hydrophilic carbon papers and vacuum-dried at 60 °C for 24 h. The mass ratio of N- Co_9S_8 or Co_9S_8 nanoparticles over Li_2S_6 is 2:8 (based on the S content), and the specific capacities were also calculated based on the weight of Sulfur in the cathodes. CR2032 coin cells were assembled in an argon-filled glove box (MBRAUN UNI lab: $\text{O}_2 < 0.1$ ppm, $\text{H}_2\text{O} < 0.1$ ppm). The electrolyte was 1.0 M lithium bis-trifluoromethanesulfonylimide (99.95% trace metals basis, Sigma-Aldrich) dissolved in 1,3-dioxolane (Sigma-Aldrich) and 1,2-dimethoxyethane (Sigma-Aldrich; 1:1 ratio by volume) with 0.1 M lithium nitrate (LiNO_3 , Sigma-Aldrich) as the additive.

Lithium metal was used as counter/reference electrode and Celgard 2400 membrane as the separator. Li_2S_6 catholyte was used as active material drop on the N- Co_9S_8 /carbon paper or Co_9S_8 /carbon paper or pure carbon paper electrodes (the sulfur mass loading is calculated according to the volume of the catholyte ≈ 1 mg cm^{-2}). The electrolyte/sulfur ratio for low sulfur mass loading (≈ 1 mg cm^{-2}) is ≈ 6 μL mg^{-1} , for high sulfur mass loading (≈ 5 mg cm^{-2}) is ≈ 4 μL mg^{-1} . The galvanostatic charge/discharge tests were carried out in the LAND CT 2001A charge/discharge system within a voltage range of 1.7–2.8 V for Li_2S_6 , and for reduction/oxidation of Li_2S , the first charge is up to 4.0 V, then charge/discharge between 1.6 and 2.8 V. The current density for Li_2S_6 tests was ranged from 0.2 to 20 A g^{-1} and for Li_2S was ranged from 0.2 to 5 A g^{-1} . The cyclic voltammogram (CV) and EIS measurements were conducted using Metrohm Auto-lab at a scan rate of 0.1 mV s^{-1} with the voltage range of 1.7–2.8 V and the frequency range was controlled from 100 kHz to 10 mHz with 10 mV fluctuations, respectively.

First-Principles Calculations: The first-principles calculations were performed based on DFT as implemented in VASP code^[64,65] to study the equilibrium structures and adsorption energy of LiPSs (Li_2S_2 and Li_2S_4 molecules) on the (311) and (440) surfaces of Co_9S_8 crystal. The projector-augmented wave (PAW) method^[66,67] was applied to treat the valence and core electrons interaction. Electron correlation and exchange effects were treated with a generalized gradient approximation (GGA) proposed by Perdew, Burke, and Ernzerhof (PBE).^[68] A cutoff-energy of 520 eV was used for the plane wave basis set. The total energy convergence criterion was 10^{-6} eV. All systems were fully relaxed until the residual Hellmann-Feynman forces were smaller than 0.01 eV \AA^{-1} . The dipole correction^[69] was considered to treat the impact of the variation of potential distribution due to the adsorption of LiPSs on (311) and (440) surfaces. In addition, the Van der Waals interactions were included during all calculations using the optB86b-vdw functional.^[70,71] The calculated lattice constant of cubic Co_9S_8 crystal is 9.79 Å, which is very close to the previously computed value of 9.80 Å.^[56] The slabs of (311) and (440) surfaces were constructed based on fully relaxed Co_9S_8 crystal, as shown in Figure 5d,e. A vacuum layer of at least 20 Å perpendicular to the plane of the 2D systems was applied to avoid the interaction between neighboring images. During the optimizations of adsorbed models, the outermost layer of slabs and LiPSs were fully relaxed, and other parts were fixed. The Brillouin zone was sampled using a $1 \times 2 \times 1$ and $2 \times 3 \times 1$ Monkhorst–Pack k -point scheme for (311) and (440) surfaces, respectively. The adsorption energy of LiPSs adsorbing on surfaces is defined as follows:

$$E_{\text{ads}} = E_{\text{LiPSs}} + E_{\text{surf}} - E_{\text{LiPSs/surf}} \quad (1)$$

where E_{LiPSs} and E_{surf} is the total energy of the LiPSs, the surface slabs, respectively. $E_{\text{LiPSs/surf}}$ is the total energy of the attached system of LiPSs and surface slab. According to Equation (1), the E_{ads} with a positive value means that the corresponding adsorption structure is energetically favorable to form. The larger the value, the easier the adsorption. It should be noted that the adsorption energy after surface doping by nitrogen atoms was also calculated.

Supporting Information

Supporting Information is available from the Wiley Online Library or from the author.

Acknowledgements

The authors are thankful to the funding from the European Research Council (ERC) under the European Union’s Horizon 2020 research and innovation program (grant agreement Nos. 714429 and 715770), and the financial support from the German Federal Ministry of Education and Research (BMBF) within the framework of the program NanoMatFutur (support code 03X5525). Dr. S.M. is grateful to Prof. Andreas Koehn for

the financial support and the support by the State of Baden-Württemberg through bwHPC.

Conflict of Interest

The authors declare no conflict of interest.

Keywords

adsorption, catalysis, Li-S batteries, lithium polysulfides, N-Co₉S₈ nanoparticles

Received: March 17, 2020

Revised: April 22, 2020

Published online: June 21, 2020

- [1] P. G. Bruce, S. A. Freunberger, L. J. Hardwick, J. M. Tarascon, *Nat. Mater.* **2012**, *11*, 19.
- [2] S. Evers, L. F. Nazar, *Acc. Chem. Res.* **2013**, *46*, 1135.
- [3] A. Manthiram, Y. Z. Fu, S. H. Chung, C. X. Zu, Y. S. Su, *Chem. Rev.* **2014**, *114*, 11751.
- [4] Y. Yang, G. Y. Zheng, Y. Cui, *Chem. Soc. Rev.* **2013**, *422*, 3018.
- [5] Y. X. Yin, S. Xin, Y. G. Guo, L. J. Wan, *Angew. Chem., Int. Ed.* **2013**, *52*, 13186.
- [6] A. Manthiram, S. H. Chung, C. X. Zu, *Adv. Mater.* **2015**, *27*, 1980.
- [7] G. M. Zhou, H. Z. Tian, Y. Jin, X. Y. Tao, B. F. Liu, R. F. Zhang, Z. W. Seh, D. Zhuo, Y. Y. Liu, J. Sun, J. Zhao, C. X. Zu, D. S. Wu, Q. F. Zhang, Y. Cui, *Proc. Natl. Acad. Sci. U. S. A.* **2017**, *114*, 840.
- [8] Z. Z. Du, X. J. Chen, W. Hu, C. H. Chuang, S. Xie, A. J. Hu, W. S. Yan, X. H. Kong, X. J. Wu, H. X. Ji, L. J. Wan, *J. Am. Chem. Soc.* **2019**, *141*, 3977.
- [9] X. L. Ji, K. T. Lee, L. F. Nazar, *Nat. Mater.* **2009**, *8*, 500.
- [10] N. Jayaprakash, J. Shen, S. S. Moganty, A. Corona, L. A. Archer, *Angew. Chem., Int. Ed.* **2011**, *50*, 5904.
- [11] G. Y. Zheng, Q. F. Zhang, J. J. Cha, Y. Yang, W. Y. Li, Z. W. Seh, Y. Cui, *Nano Lett.* **2013**, *13*, 1265.
- [12] G. M. Zhou, L. C. Yin, D. W. Wang, L. Li, S. F. Pei, I. R. Gentle, F. Li, H. M. Cheng, *ACS Nano* **2013**, *7*, 5367.
- [13] J. Zhang, C. P. Yang, Y. X. Yin, L. J. Wan, Y. G. Guo, *Adv. Mater.* **2016**, *28*, 9539.
- [14] S. Moon, Y. H. Jung, W. K. Jung, D. S. Jung, J. W. Choi, D. K. Kim, *Adv. Mater.* **2013**, *25*, 6547.
- [15] X. Liang, C. Hart, Q. Pang, A. Garsuch, T. Weiss, L. F. Nazar, *Nat. Commun.* **2015**, *6*, 5682.
- [16] S. Xin, L. Gu, N. H. Zhao, Y. X. Yin, L. J. Zhou, Y. G. Guo, L. J. Wan, *J. Am. Chem. Soc.* **2012**, *134*, 18510.
- [17] Q. Z. Zhu, Q. Zhao, Y. B. An, B. Anasori, H. R. Wang, B. Xu, *Nano Energy* **2017**, *33*, 402.
- [18] J. X. Song, T. Xu, M. L. Gordin, P. Y. Zhu, D. P. Lv, Y. B. Jiang, Y. S. Chen, Y. H. Duan, D. H. Wang, *Adv. Funct. Mater.* **2014**, *24*, 1243.
- [19] K. A. See, Y. S. Jun, J. A. Gerbec, J. K. Sprafke, F. Wudl, G. D. Stucky, R. Seshadri, *ACS Appl. Mater. Interfaces* **2014**, *6*, 10908.
- [20] Z. Y. Wang, Y. F. Dong, H. J. Li, Z. B. Zhao, H. B. Wu, C. Hao, S. H. Liu, J. S. Qiu, X. W. Lou, *Nat. Commun.* **2014**, *5*, 5002.
- [21] G. M. Zhou, E. Paek, G. S. Hwang, A. Manthiram, *Nat. Commun.* **2015**, *6*, 7760.
- [22] Q. Pang, D. Kundu, M. Cuisinier, L. F. Nazar, *Nat. Commun.* **2014**, *5*, 4759.
- [23] X. Y. Tao, J. G. Wang, C. Liu, H. T. Wang, H. B. Yao, G. Y. Zheng, Z. W. Seh, Q. X. Cai, W. Y. Li, G. M. Zhou, C. X. Zu, Y. Cui, *Nat. Commun.* **2016**, *7*, 11203.
- [24] Z. W. Seh, J. H. Yu, W. Y. Li, P. C. Hsu, H. T. Wang, Y. M. Sun, H. B. Yao, Q. F. Zhang, Y. Cui, *Nat. Commun.* **2014**, *5*, 5017.
- [25] Q. Pang, D. Kundu, L. F. Nazar, *Mater. Horiz.* **2016**, *3*, 130.
- [26] Z. Yuan, H. J. Peng, T. Z. Hou, J. Q. Huang, C. M. Chen, D. W. Wang, X. B. Cheng, F. Wei, Q. Zhang, *Nano Lett.* **2016**, *16*, 519.
- [27] Z. M. Cui, C. X. Zu, W. D. Zhou, A. Manthiram, J. B. Goodenough, *Adv. Mater.* **2016**, *28*, 6926.
- [28] X. Liang, A. Garsuch, L. F. Nazar, *Angew. Chem., Int. Ed.* **2015**, *54*, 3907.
- [29] H. B. Yao, G. Y. Zheng, P. C. Hsu, D. S. Kong, J. J. Cha, W. Y. Li, Z. W. Seh, M. T. McDowell, K. Yan, Z. Liang, V. K. Narasimhan, Y. Cui, *Nat. Commun.* **2014**, *5*, 3943.
- [30] L. L. Zhang, D. B. Liu, Z. Muhammad, F. Wan, W. Xie, Y. J. Wang, L. Song, Z. Q. Niu, J. Chen, *Adv. Mater.* **2019**, *31*, 1903955.
- [31] G. Babu, N. Masurkar, H. Al Salem, L. M. R. Arave, *J. Am. Chem. Soc.* **2017**, *139*, 171.
- [32] S. Z. Huang, Y. Wang, J. P. Hu, Y. V. Lim, D. Z. Kong, Y. Zheng, M. Ding, M. E. Pam, H. Y. Yang, *ACS Nano* **2018**, *12*, 9504.
- [33] L. L. Zhang, X. Chen, F. Wan, Z. Q. Niu, Y. J. Wang, Q. Zhang, J. Chen, *ACS Nano* **2018**, *12*, 9578.
- [34] M. Chhowalla, H. S. Shin, G. Eda, L. J. Li, K. P. Loh, H. Zhang, *Nat. Chem.* **2013**, *5*, 263.
- [35] X. X. Zou, X. X. Huang, A. Goswami, R. Silva, B. R. Sathe, E. Mikmeková, T. Asefa, *Angew. Chem., Int. Ed.* **2014**, *53*, 4372.
- [36] J. H. Hao, W. S. Yang, Z. Peng, C. Zhang, Z. P. Huang, W. D. Shi, *ACS Catal.* **2017**, *7*, 4214.
- [37] Q. Pang, J. T. Tang, H. Huang, X. Liang, C. Hart, K. C. Tam, L. F. Nazar, *Adv. Mater.* **2015**, *27*, 6021.
- [38] T. Z. Hou, W. T. Xu, X. Chen, H. J. Peng, J. Q. Huang, Q. Zhang, *Angew. Chem., Int. Ed.* **2017**, *56*, 8178.
- [39] L. C. Yin, J. Liang, G. M. Zhou, F. Li, R. Saito, H. M. Cheng, *Nano Energy* **2016**, *25*, 203.
- [40] G. Q. Tan, R. Xu, Z. Y. Xing, Y. F. Yuan, J. Lu, J. G. Wen, C. Liu, L. Ma, C. Zhan, Q. Liu, T. P. Wu, Z. L. Jian, R. Shahbazian-Yassar, Y. Ren, D. J. Miller, L. A. Curtiss, X. L. Ji, K. Amine, *Nat. Energy* **2017**, *2*, 17090.
- [41] Y. Zhou, D. Yan, H. Xu, J. Feng, X. Jiang, J. Yue, J. Yang, Y. Qian, *Nano Energy* **2015**, *12*, 528.
- [42] J. K. Chang, C. M. Wu, I. W. Sun, *J. Mater. Chem.* **2010**, *20*, 3729.
- [43] M. S. Faber, R. Dziedzic, M. A. Lukowski, N. S. Kaiser, Q. Ding, S. Jin, *J. Am. Chem. Soc.* **2014**, *136*, 10053.
- [44] Y. Z. Song, W. Zhao, L. Kong, L. Zhang, X. Y. Zhu, Y. L. Shao, F. Ding, Q. Zhang, J. Y. Sun, Z. F. Liu, *Energy Environ. Sci.* **2018**, *11*, 2620.
- [45] F. Pei, L. L. Lin, D. H. Ou, Z. M. Zheng, S. G. Mo, X. L. Fang, N. F. Zheng, *Nat. Commun.* **2017**, *8*, 482.
- [46] Z. H. Sun, J. Q. Zhang, L. C. Yin, G. J. Hu, R. P. Fang, H. M. Cheng, F. Li, *Nat. Commun.* **2017**, *8*, 14627.
- [47] L. Li, L. Chen, S. Mukherjee, J. Gao, H. Sun, Z. B. Liu, X. L. Ma, T. Gupta, C. V. Singh, W. C. Ren, H. M. Cheng, N. Koratkar, *Adv. Mater.* **2017**, *29*, 1602734.
- [48] F. Zhou, Z. Li, X. Luo, T. Wu, B. Jiang, L. L. Lu, H. B. Yao, M. Antonietti, S. H. Yu, *Nano Lett.* **2018**, *18*, 1035.
- [49] J. T. Zhang, Z. Li, Y. Chen, S. Y. Gao, X. W. Lou, *Angew. Chem., Int. Ed.* **2018**, *57*, 10944.
- [50] H. B. Lin, S. L. Zhang, T. R. Zhang, H. L. Ye, Q. F. Yao, G. W. Zheng, J. Y. Lee, *Adv. Energy Mater.* **2018**, *8*, 1801868.
- [51] Q. H. Yu, Y. Lu, R. J. Luo, X. M. Liu, K. F. Huo, J. K. Kim, J. He, Y. S. Luo, *Adv. Funct. Mater.* **2018**, *28*, 1804520.
- [52] D. W. Su, M. Cortie, G. X. Wang, *Adv. Energy Mater.* **2017**, *7*, 1602014.
- [53] L. Kong, X. Chen, B. Q. Li, H. J. Peng, J. Q. Huang, J. Xie, Q. Zhang, *Adv. Mater.* **2018**, *30*, 1705219.

- [54] G. R. Li, W. Lei, D. Luo, Y. P. Deng, Z. P. Deng, D. L. Wang, A. P. Yu, Z. W. Chen, *Energy Environ. Sci.* **2018**, *11*, 2372.
- [55] H. Q. Jiang, X. C. Liu, Y. S. Wu, Y. F. Shu, X. Gong, F. S. Ke, H. X. Deng, *Angew. Chem., Int. Ed.* **2018**, *57*, 3916.
- [56] C. L. Dai, J. M. Lim, M. Q. Wang, L. Y. Hu, Y. M. Chen, Z. Y. Chen, H. Chen, S. J. Bao, B. L. Shen, Y. Li, G. Henkelman, M. W. Xu, *Adv. Funct. Mater.* **2018**, *28*, 1704443.
- [57] K. P. Cai, M. K. Song, E. J. Cairns, Y. G. Zhang, *Nano Lett.* **2012**, *12*, 6474.
- [58] Y. Yang, M. T. McDowell, A. Jackson, J. J. Cha, S. S. Hong, Y. Cui, *Nano Lett.* **2010**, *10*, 1486.
- [59] Z. F. Deng, Z. A. Zhang, Y. Q. Lai, J. Liu, J. Li, Y. X. Liu, *J. Electrochem. Soc.* **2013**, *160*, A553.
- [60] J. Park, B. C. Yu, J. S. Park, J. W. Choi, C. Kim, Y. E. Sung, J. B. Goodenough, *Adv. Energy Mater.* **2017**, *7*, 1602567.
- [61] C. Ho, I. D. Raistrick, R. A. Huggins, *J. Electrochem. Soc.* **1980**, *127*, 343.
- [62] X. X. Zuo, C. J. Fan, X. Xiao, J. S. Liu, J. M. Nan, *J. Power Sources* **2012**, *219*, 94.
- [63] Y. S. Jung, P. Lu, A. S. Cavanagh, C. Ban, G. H. Kim, S. H. Lee, S. M. George, S. J. Harris, A. C. Dillon, *Adv. Energy Mater.* **2013**, *3*, 213.
- [64] G. Kresse, J. Furthmuller, *Phys. Rev. B* **1996**, *54*, 11169.
- [65] G. Kresse, J. Furthmuller, *Comput. Mater. Sci.* **1996**, *6*, 15.
- [66] P. E. Blochl, *Phys. Rev. B* **1994**, *50*, 17953.
- [67] G. Kresse, D. Joubert, *Phys. Rev. B* **1999**, *59*, 1758.
- [68] J. P. Perdew, K. Burke, M. Ernzerhof, *Phys. Rev. Lett.* **1996**, *77*, 3865.
- [69] L. Bengtsson, *Phys. Rev. B* **1999**, *59*, 12301.
- [70] J. Klimes, D. R. Bowler, A. Michaelides, *J. Phys.: Condens. Matter* **2010**, *22*, 022201.
- [71] J. Klimes, D. R. Bowler, A. Michaelides, *Phys. Rev. B* **2011**, *83*, 195131.